


Generation of Optical Frequency Comb via Giant Optomechanical Oscillation

Yong Hu,^{1,*} Shulin Ding,^{1,*} Yingchun Qin,¹ Jiaxin Gu,¹ Wenjie Wan,² Min Xiao,^{1,3} and Xiaoshun Jiang^{1,†}

¹National Laboratory of Solid State Microstructures, College of Engineering and Applied Sciences, School of Physics, and Collaborative Innovation Center of Advanced Microstructures, Nanjing University, Nanjing 210093, China

²The State Key Laboratory of Advanced Optical Communication Systems and Networks, University of Michigan-Shanghai Jiao Tong University Joint Institute, Shanghai Jiao Tong University, Shanghai 200240, China

³Department of Physics, University of Arkansas, Fayetteville, Arkansas 72701, USA

 (Received 16 December 2020; accepted 5 August 2021; published 20 September 2021)

Optical frequency combs (OFCs) are essential in precision metrology, spectroscopy, distance measurement, and optical communications. Significant advances have been made recently in achieving micro-OFC devices based on parametric frequency conversion or electro-optic phase modulation. Here, we demonstrate a new kind of microcomb using a cavity optomechanical system with giant oscillation amplitude. We observe both optical and microwave frequency combs in a microtoroid resonator, which feature a flat OFC with 938 comb lines and a repetition rate as low as 50.22 MHz, as well as a flat microwave frequency comb with 867 comb lines. To generate such giant oscillation amplitude, we excite an overcoupled optical mode with a large blue detuning that is assisted with the thermo-optic nonlinearity. A new type of nonlinear oscillation, induced by competition between the optomechanical oscillation and thermo-optic nonlinearity, is also observed.

DOI: [10.1103/PhysRevLett.127.134301](https://doi.org/10.1103/PhysRevLett.127.134301)

Introduction.—Optical frequency combs (OFCs) are widely used in optical metrology, precision spectroscopy, optical clock and radio frequency (rf) photonics [1,2]. Such frequency combs can be generated by mode-locked femtosecond lasers [3,4], electro-optic (EO) modulation of a continuous-wave laser [5], or parametric oscillations with intrinsic material nonlinearities (e.g., Kerr microcomb) [6,7]. In comparison to the traditional mode-locked OFCs [3,4], the Kerr microcombs typically exhibit high repetition rates and are suitable for on-chip integration [5–7], which make them desirable for coherent optical communications [8], ultrafast optical ranging [9], and astronomical spectrograph calibration [10,11], as well as low-noise microwave and terahertz generations [12,13]. Nevertheless, OFCs with lower repetition rates (< 1 GHz) are desirable for certain applications such as high-resolution spectroscopy [14,15], sensing [16], pump source for generating multiphoton entangled states [17], and high-power supercontinuum generation [18]. Although OFCs with such low repetition rates can be easily obtained in traditional mode-locked laser frequency combs using Ti:sapphire or fiber lasers, it would be challenging for the chip-based optical microcombs (Kerr [6,7] or EO microcombs [19]) to have such low repetition rates, since the optical microresonators have to be very large while maintaining very high-quality (high- Q) factors. Recently, a Kerr soliton microcomb with the repetition rate as low as 1.859 GHz has been reported using a 35-mm-diameter silica microdisk resonator [20].

Parallel to the OFCs, frequency combs in the microwave region (i.e., microwave frequency comb, MFC) can be used in multichannel microwave radars [21], arbitrary waveform generations [22], and Doppler reflectometry [23]. So far, MFCs have been realized by various methods, such as using a frequency-locked semiconductor laser [24,25] or focusing ultrafast laser pulses onto a tunneling junction [26]. In spite of the broadband and narrow linewidth of these demonstrations [25,26] on MFCs, they are subject to complicated setups.

At the same time, optomechanical effects based on microresonators have promised a variety of potential applications in the past decade [27,28]. Among them, several schemes to produce OFCs via the generations of high-order harmonics of mechanical modes were theoretically proposed [29–32]. Different from the optical Kerr frequency combs, the repetition rate of the optomechanical OFC does not directly depend on the microcavity size but on the mechanical oscillation frequency, which makes it promising for the generations of chip-based OFCs with lower repetition rates. However, to date, OFCs based on such optomechanical oscillations have only been observed experimentally with very limited comb lines [33,34] due to the small mechanical oscillation amplitude. One big challenge for demonstrating OFC in the cavity optomechanical systems stems from the appearance of chaos [35–39] with a high pump power. In addition, optomechanical oscillation has also been demonstrated for rf harmonics (i.e., MFC)

generations [40–43]. Although the optomechanical MFC with a bandwidth up to 6.9 GHz has been obtained [43], both the spectra of the optomechanical generated OFC [34] and MFC are not flat and have limited comb lines, which further limit their applications [14–16,21,22].

Here, we experimentally and theoretically demonstrate the generations of both OFC and MFC via giant optomechanical oscillation (OMO) in a high- Q chip-based silica microresonator. We have achieved a flat OFC with 938 optical comb lines and a repetition rate of 50.22 MHz. By properly operating the optical mode, we have successfully inhibited the emergence of optomechanical chaos even at a very high input pump power. Also, a narrow-linewidth and flat MFC is obtained with a comb span as broad as 43.5 GHz. Additionally, we have experimentally observed and theoretically explained a new kind of dynamical phenomenon caused by the competition between the OMO and the thermo-optic nonlinearity in the microresonator.

Results.—The schematic diagram of the cavity optomechanical system [33] is shown in Fig. 1(a). A fiber-taper-coupled high- Q silica whispering-gallery-mode microcavity is employed as an optomechanical platform. The mechanical oscillation is driven by exciting a high- Q optical mode with a blue-detuned pump. In our model, the

cavity optomechanical dynamics is further regulated by thermo-optic effect [44]. The optical mode, the mechanical displacement, and the average temperature difference evolve following the equations (see the Supplemental Material [45]).

$$\frac{da}{dt} = [-i(\Delta\omega_L + Gx - \beta_T\Delta T) - \frac{\kappa}{2}]a + \sqrt{\kappa_e}s_{in}, \quad (1)$$

$$\frac{d^2x}{dt^2} + \Gamma_m \frac{dx}{dt} + \Omega_m^2 x = \frac{G}{m\omega_0} |a|^2, \quad (2)$$

$$\frac{d\Delta T}{dt} = -\gamma_T \Delta T + c_T |a|^2. \quad (3)$$

Here, a is the amplitude of the optical field in the cavity ($|a|^2$ represents the cavity energy); $\Delta\omega_L = \omega_L - \omega_0$ is the frequency detuning between the pump laser frequency ω_L and the resonant cavity frequency ω_0 . x is the displacement of the cavity, ΔT is the average temperature difference between the optical field location and the surrounding, and $G = -\partial\omega_0/\partial x$ is the optomechanical coupling coefficient between the mechanical mode and the optical modes. $\kappa = \kappa_0 + \kappa_e$ is the total optical decay rate with κ_0 and κ_e being, respectively, the intrinsic decay rate and the external coupling decay rate between the cavity and the tapered fiber, while s_{in} is the amplitude of the input pump field. Γ_m , m , and Ω_m are, respectively, the intrinsic mechanical decay rate, effective mass, and the resonant frequency of the mechanical oscillator. β_T is the coefficient of the resonant frequency drift induced by temperature variation, γ_T is the thermal relaxation rate of the resonator, and $c_T = \alpha_T \gamma_T / \beta_T$ characterizes the thermo-optic effect with light absorption (α_T is the coefficient of frequency drift induced by light absorption). To acquire the form of OFC, we assume that the displacement $x(t)$ carries out a sinusoidal motion [51]; i.e., $x(t) = X_0 + X_1 \sin \Omega_m t$, where X_0 and X_1 are, respectively, the mean value and the amplitude of the mechanical oscillation displacement. The solution of the optical field amplitude in the cavity can be written as a Fourier series, $a(t) = \sum_k a_k e^{ik\Omega_m t}$ with

$$a_k = \sum_n \frac{i^k J_{k-n}(\beta) J_n(-\beta)}{i(n\omega_m + \Delta\omega_{\text{eff}} + GX_0) + \kappa/2} \sqrt{\kappa_e} s_{in}, \quad (4)$$

where a_k stands for k th optical sideband, $J_n(\beta)$ is the n th order Bessel function of the first kind, and $\beta = GX_1/\Omega_m$ is defined as the effective mechanical amplitude of the OMO. $\Delta\omega_{\text{eff}} = \omega_L - \omega_c$ is the effective pump frequency detuning [52] under the consideration of thermo-optic effect and ω_c denotes center resonant frequency of the oscillating cavity [Fig. 1(b)].

Based on Eq. (4), the span of the OFC can be approximately estimated to be $2\beta\Omega_m$, which is proportional to the mechanical oscillation amplitude. Therefore, to generate more sidebands, one of the practical methods is to enhance

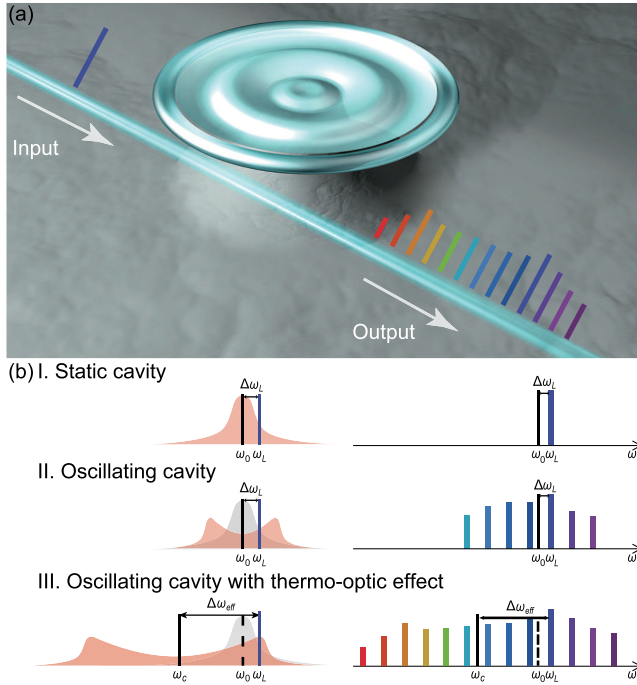


FIG. 1. Schematic diagram and principle of the OFC generation with giant optomechanical oscillation. (a) Schematic diagram of optomechanical frequency comb. (b) Illustration of optomechanical frequency comb span expansion assisted by thermo-optic effect. Left: cavity spectrum. I, static cavity; II, oscillating cavity; III, oscillating cavity with thermo-optic effect. Right: corresponding OFC spectra.

the amplitude of the mechanical oscillation by directly increasing the pump power. Here, we demonstrate that broader optical combs can be obtained with a large blue-detuned pump at certain optical power. This large blue frequency detuning is achieved by the interplay between the OMO and thermo-optic nonlinearity. The physical pictures of such interplay and OFC generation are depicted in Fig. 1(b). When the system operates below the oscillation threshold, the transmission spectrum of the optical mode exhibits a symmetric Lorentzian profile [Fig. 1(b), curve I]. However, when above the threshold, the displacement of the mechanical oscillator will modulate the optical mode by periodically expanding and compressing the microcavity through dynamic backaction [53]. Thus, this periodic but highly nonlinear modulation gives rise to many harmonics around the pump frequency at $\omega_L + k\Omega_m$, where $k = \pm 1, \pm 2, \dots$. Once the mechanical oscillation is established, the transmission spectrum of the optical mode will be broadened [Fig. 1(b), curve II], and several comb lines will appear in the frequency domain. Then, due to the optical energy difference between the static and the oscillating cavity modes, the accumulated heat due to photon absorption (i.e., thermo-optic effect) in the cavity will induce a redshift for the cavity resonance, which results in an increase of the effective pump detuning. According to our theoretical model, we find that gradually increasing the effective pump detuning will amplify the mechanical amplitude due to the increased optical radiation pressure for an oscillating cavity [54,55] [also see the Supplemental Material [45], Figs. S1(a) and S1(b)]. Owing to the enhanced mechanical oscillation, more sidebands are generated and the oscillating cavity spectrum is further broadened [Fig. 1(b), curve III].

The experimental setup for the generation of the OFC is shown in Fig. S8 of the Supplemental Material [45]. Here, we use a chip-based silica microtoroid cavity (Supplemental Material [45], Sec. IV) with a diameter of $61.3 \mu\text{m}$. The measured intrinsic optical Q factor is 1.13×10^8 , and the mechanical Q factor is 5473 for a radial-breathing mode of 50.08 MHz. To enlarge the mechanical oscillation amplitude, the optical mode is deeply overcoupled with a total optical decay rate approximately equaling the mechanical oscillation angular frequency (Supplemental Material [45], Sec. III) by reducing the gap between the fiber taper and the microcavity. Note that this coupling condition makes our system not work in the resolved-sideband regime, which is also helpful to avoid the radiation pressure induced chaos [35]. By exciting the overcoupled optical mode with a large blue-detuned pump, we achieve an optomechanical OFC with 938 comb lines under a pump power of 448 mW [Fig. 2(a)]. The typical OFC output is detected by an optical spectrum analyzer with a spectral resolution of 5 MHz. In the frequency range from -30.5 to -7.5 GHz [Fig. 2(a)], over 450 comb lines are observed within 10 dB power variation,

which indicates the high spectral flatness of the generated OFC. This flatness feature can be mainly attributed to the high optical Q factor of the silica microcavity (Supplemental Material [45], Sec. III). By importing the optical signal into a fast photodetector (38 GHz) followed by an oscilloscope (10 GHz) and an electrical spectrum analyzer (43.5 GHz), we can experimentally generate and detect a broadband MFC that is resulted from the beat notes of the OFC teeth. Because of the large oscillation amplitude of the mechanical oscillator and the flat spectrum of the generated OFC [Fig. 2(b)], we have achieved a MFC that exhibits 867 comb lines with a span of about 43.5 GHz [Fig. 2(b)], which is much broader and flatter than the one reported in the previous work [43]. Owing to the high- Q factor of the mechanical mode and giant mechanical oscillation [56], the linewidths (full width at half maximum) of the MFC teeth are very narrow. The measured linewidth is as narrow as 1.09 Hz [Fig. 2(d)] for the first comb line, 6.24 Hz for the 20th comb line, and 4.12 kHz for the 600th comb line (Supplemental Material [45], Fig. S11). The repetition rate of the MFC is equal to that of the OFC, since both rely solely on the mechanical oscillation frequency. To further characterize our OFC, we have also measured the phase noise and Allan deviations of the repetition rate (Supplemental Material [45], Sec. V), which indicate the high performance of our OFC. Moreover, we have performed detailed numerical simulations on the generated spectra of the OFC and MFC based

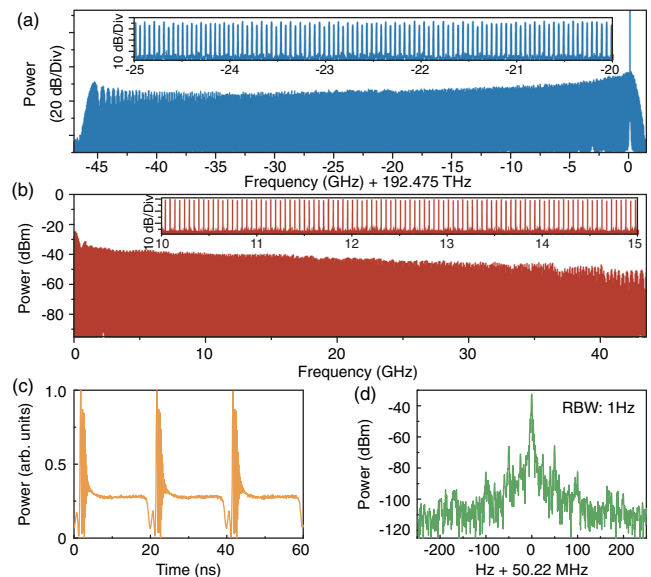


FIG. 2. Representative curves of the observed optomechanical frequency comb and its experimental characterizations. (a) Typically observed OFC. (b) Typical MFC revealed in rf spectrum with the repetition rate exactly coinciding with the mechanical oscillation frequency $\Omega_m/2\pi$. (c) Time domain periodical optical pulse train. (d) The measured rf spectrum of the oscillated mechanical mode. RBW: resolution bandwidth.

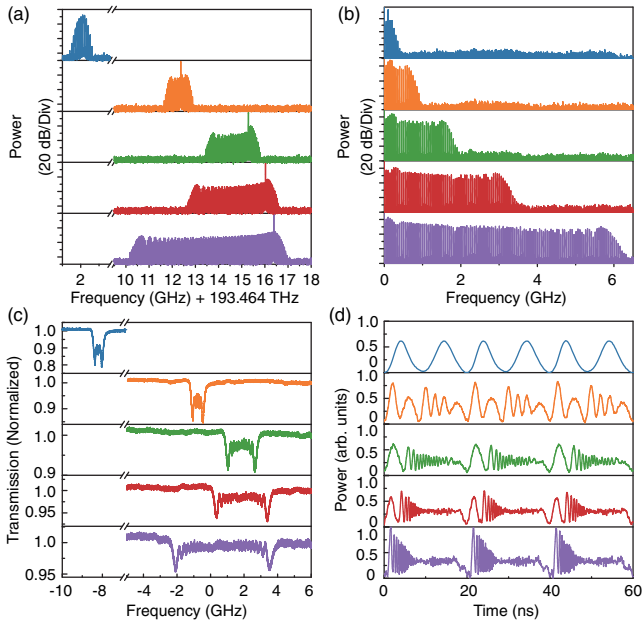


FIG. 3. Evolutions of OFC and MFC as a function of the pump frequency. (a) Optical spectra. (b) Radio frequency spectra. (c) Transmission spectra of the probe light mediated by mechanical oscillation. (d) Transmitted optical power versus time. The curves of the same color indicate the results of the same pump frequency.

on our model (Supplemental Material [45], Fig. S5), which agree very well with the experimentally measured results.

To better understand the optomechanical combs, we carefully monitor the evolutions of the OFC and MFC spectra, as well as the corresponding transmission spectra of the probe light, by selecting different pump frequencies, as shown in Figs. 3(a)–3(c), at a fixed pump power of 14.4 mW. The measured optical and rf spectra are presented in Figs. 3(a) and 3(b), respectively. In Fig. 3(a), by increasing the pump frequency, more OFC comb lines appear at the longer wavelength side of the pump light, which stems from the increased blue pump detuning caused by thermo-optic effect [Supplemental Material [45], Fig. S1(b)]. Accordingly, more spectral lines emerge in the spectrum of MFC [Fig. 3(b)]. The corresponding transmitted optical power signals at different pump frequencies are presented in Fig. 3(d). During the pump frequency increasing, the output signal first shows a sinusoidal-like waveform and then gradually changes to be a train of decay peaks with only one series per period [57]. This temporal behavior of having a single series of decay peaks is different from the previously predicted results [29,58] that exhibit two main peaks per period under high power pump. To characterize such optomechanically oscillating cavity, we further measure the transmission spectrum of the cavity by launching a counterpropagating probe light into the microcavity. Figure 3(c) displays the transmission spectra of the probe light, which shows a

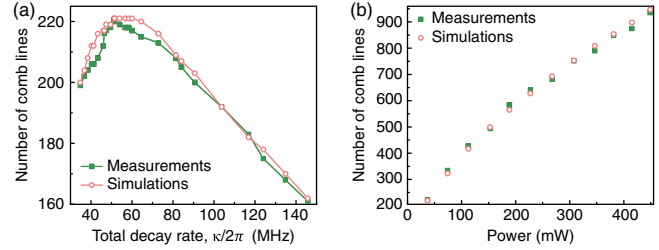


FIG. 4. Measured and simulated number of comb lines. (a) Number of the comb lines as a function of the cavity decay rate. (b) Number of the comb lines as a function of the pump power. The data with solid symbols are measured results and those with opened ones are numerically simulated results.

series of overlapped resonant dips [54,59] instead of a single resonant dip belonging to the static cavity. Numerical studies on the comb evolutions are also carried out (Supplemental Material [45], Fig. S6), which led to excellent matches with our experimental results.

In the experiment, we have also investigated the dependence between the number of the generated optical comb lines and the total cavity decay rate with a fixed pump power (37.5 mW) by changing the coupling distance between the fiber taper and the microcavity. As shown in Fig. 4(a), the number of generated comb lines increases first with increasing total decay rate and then gradually decreases as the total decay rate becomes larger than a value ($\sim 2\pi \times 51$ MHz) close to the mechanical oscillation angular frequency, which agrees with the theoretical (Supplemental Material [45], Sec. III) and numerical analyses. In addition, the OFC generation also depends on the input pump power. To achieve a broadband OFC, we have carefully examined the evolution of the OFC in terms of different pump powers with optimized pump frequencies while keeping the coupling strength ($\kappa \sim 2\pi \times 60$ MHz) between the fiber taper and the microcavity fixed. Figure 4(b) shows the number of the generated comb lines as a function of input pump power, which increases with the growing pump power and agrees well with the numerically simulated results. Such a relationship offers a promising way to further expand the comb span with a high pump power. In the experiment, we have demonstrated the wavelength tunability of our OFCs with a total working span of 1.42 nm (Supplemental Material [45], Fig. S12) by controlling the temperature of the sample and using different optical modes, which indicates that our OFC may be useful for frequency-agile dual-comb spectroscopy [60]. During the measurement, the optomechanical chaotic effect [35,37] is not observed, which may be due to the strong overcoupling of the optical mode and the large Q factor of the mechanical mode.

Additionally, we intriguingly observed a new dynamical phenomenon (Fig. 5) with another optical mode [Supplemental Material [45], Figs. S8(d)–S8(f)] of the

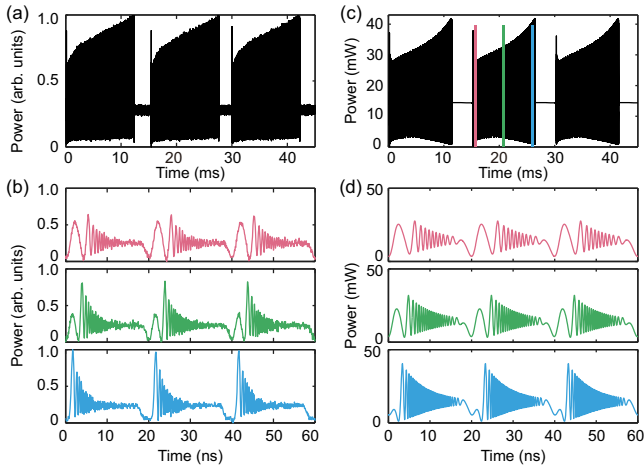


FIG. 5. Time traces of the OMTO. (a),(b) Experimental results (a) in the slow timescale and (b) three typical snapshots in the fast timescale. (c),(d) Numerical results. The calculated time trace with slow timescale is shown in (c), while three fast time traces [corresponding to the marked times in (c)] are shown in (d).

same sample in a certain pump frequency region, named optomechanical-thermo-oscillation (OMTO) here, which is caused by the competition between OMO and thermo-optic nonlinearity (see the Supplemental Material [45] for details, Sec. I). This OMTO can be considered as a slow-fast dynamic process [61], since the response of OMO is much faster than that of the thermal dynamics. We have further identified clearly distinguishable slow and fast oscillation periods [Figs. 5(a) and 5(b)] in this OMTO. The slow period of the recorded OMTO is in the range from several milliseconds to tens of milliseconds in the experimental observations, which is related to the thermal relaxation time of the sample and the pump detuning. The fast period is equal to the mechanical oscillation period of about 19.96 ns. The corresponding numerical simulations on the OMTO are shown in Figs. 5(c) and 5(d), which agree well with the experimental results.

Conclusions.—We have demonstrated the generations of both optical and microwave frequency microcombs in the same cavity optomechanical system. Using optomechanical effects to generate microsized OFCs and MFCs has added a new platform to produce versatile and highly integrated frequency combs. Owing to the giant mechanical oscillation amplitude induced by large blue-detuned pump, we have obtained an OFC with 938 comb lines and a MFC with 867 comb lines with a 50.22-MHz repetition rate in a chip-based microresonator. Also, we have demonstrated the wavelength tunability of our OFC. Despite the relatively narrow optical spectrum observed here, the bandwidth of our OFCs is already enough (or close to) for certain unique applications such as single comb atomic spectroscopy [15], dual-comb molecular spectroscopy [60,62], refractive index sensors [16], and pump sources for generating multiphoton entangled states [17]. In fact, the

spectral range can be expanded by further optimizing the parameters of the system, such as increasing both the optical and mechanical Q factors and decreasing the effective motional mass. The generated microwave frequency microcombs with high coherence and broad bandwidth may find applications in microwave communications or specific waveform generation.

We thank Professor Kerry Vahala for helpful discussions. This research was supported by the National Key R&D Program of China (2016YFA0302500, 2017YFA 0303703), the National Natural Science Foundation of China (NSFC) (61922040), Guangdong Major Project of Basic and Applied Basic Research (2020B0301030009), and the Fundamental Research Funds for the Central Universities (021314380189).

*Y. H. and S. D. contributed equally to this work.

†jxs@nju.edu.cn

- [1] T. Udem, R. Holzwarth, and T. W. Hänsch, Optical frequency metrology, *Nature (London)* **416**, 233 (2002).
- [2] T. J. Kippenberg, R. Holzwarth, and S. A. Diddams, Microresonator-based optical frequency combs, *Science* **332**, 555 (2011).
- [3] D. J. Jones, S. A. Diddams, J. K. Ranka, A. Stentz, R. S. Windeler, J. L. Hall, and S. T. Cundiff, Carrier-envelope phase control of femtosecond mode-locked lasers and direct optical frequency synthesis, *Science* **288**, 635 (2000).
- [4] R. Holzwarth, T. Udem, T. W. Hänsch, J. C. Knight, W. J. Wadsworth, and P. S. J. Russell, Optical Frequency Synthesizer for Precision Spectroscopy, *Phys. Rev. Lett.* **85**, 2264 (2000).
- [5] A. Parriaux, K. Hammani, and G. Millot, Electro-optic frequency combs, *Adv. Opt. Photonics* **12**, 223 (2020).
- [6] T. J. Kippenberg, A. L. Gaeta, M. Lipson, and M. L. Gorodetsky, Dissipative Kerr solitons in optical microresonators, *Science* **361**, eaan8083 (2018).
- [7] A. L. Gaeta, M. Lipson, and T. J. Kippenberg, Photonic-chip-based frequency combs, *Nat. Photonics* **13**, 158 (2019).
- [8] J. Pfeifle *et al.*, Coherent terabit communications with microresonator Kerr frequency combs, *Nat. Photonics* **8**, 375 (2014).
- [9] P. Trocha *et al.*, Ultrafast optical ranging using microresonator soliton frequency combs, *Science* **359**, 887 (2018).
- [10] E. Obrzud *et al.*, A microphotonic astrocomb, *Nat. Photonics* **13**, 31 (2019).
- [11] M.-G. Suh *et al.*, Searching for exoplanets using a microresonator astrocomb, *Nat. Photonics* **13**, 25 (2019).
- [12] J. Li, X. Yi, H. Lee, S. A. Diddams, and K. J. Vahala, Electro-optical frequency division and stable microwave synthesis, *Science* **345**, 309 (2014).
- [13] W. Liang, D. Eliyahu, V. S. Ilchenko, A. A. Savchenkov, A. B. Matsko, D. Seidel, and L. Maleki, High spectral purity Kerr frequency comb radio frequency photonic oscillator, *Nat. Commun.* **6**, 7957 (2015).

- [14] N. Picqué and T. W. Hänsch, Frequency comb spectroscopy, *Nat. Photonics* **13**, 146 (2019).
- [15] N. Wilson, N. B. Hébert, C. Perrella, P. Light, J. Genest, S. Pustelny, and A. Luiten, Simultaneous Observation of Nonlinear Magneto-Optical Rotation in the Temporal and Spectral Domains with an Electro-Optic Frequency Comb, *Phys. Rev. Applied* **10**, 034012 (2018).
- [16] Y. Bao, X. Yi, Z. Li, Q. Chen, J. Li, X. Fan, and X. Zhang, A digitally generated ultrafine optical frequency comb for spectral measurements with 0.01-pm resolution and 0.7- μ s response time, *Light Sci. Appl.* **4**, e300 (2015).
- [17] C. Reimer *et al.*, Generation of multiphoton entangled quantum states by means of integrated frequency combs, *Science* **351**, 1176 (2016).
- [18] P. A. Champert, S. V. Popov, and J. R. Taylor, Generation of multiwatt, broadband continua in holey fibers, *Opt. Lett.* **27**, 122 (2002).
- [19] M. Zhang, B. Buscaino, C. Wang, A. Shams-Ansari, C. Reimer, R. Zhu, J. M. Kahn, and M. Lončar, Broadband electro-optic frequency comb generation in a lithium niobate microring resonator, *Nature (London)* **568**, 373 (2019).
- [20] M.-G. Suh and K. Vahala, Gigahertz-repetition-rate soliton microcombs, *Optica* **5**, 65 (2018).
- [21] B. Nuss, J. Mayer, S. Marahrens, and T. Zwick, Frequency comb OFDM radar system with high range resolution and low sampling rate, *IEEE Trans. Microwave Theory Tech.* **68**, 3861 (2020).
- [22] S. Fukushima, C. F. C. Silva, Y. Muramoto, and A. J. Seeds, Optoelectronic millimeter-wave synthesis using an optical frequency comb generator, optically injection locked lasers, and a unitraveling-carrier photodiode, *J. Lightwave Technol.* **21**, 3043 (2003).
- [23] T. Tokuzawa *et al.*, Microwave frequency comb Doppler reflectometer applying fast digital data acquisition system in LHD, *Rev. Sci. Instrum.* **89**, 10H118 (2018).
- [24] S.-C. Chan, G.-Q. Xia, and J.-M. Liu, Optical generation of a precise microwave frequency comb by harmonic frequency locking, *Opt. Lett.* **32**, 1917 (2007).
- [25] Y.-S. Juan and F.-Y. Lin, Ultra broadband microwave frequency combs generated by an optical pulse-injected semiconductor laser, *Opt. Express* **17**, 18596 (2009).
- [26] M. J. Hagmann, A. J. Taylor, and D. A. Yarotski, Observation of 200th harmonic with fractional linewidth of 10^{-10} in a microwave frequency comb generated in a tunneling junction, *Appl. Phys. Lett.* **101**, 241102 (2012).
- [27] T. J. Kippenberg and K. J. Vahala, Cavity optomechanics: Back-action at the mesoscale, *Science* **321**, 1172 (2008).
- [28] M. Aspelmeyer, T. J. Kippenberg, and F. Marquardt, Cavity optomechanics, *Rev. Mod. Phys.* **86**, 1391 (2014).
- [29] M.-A. Miri, G. D'Aguanno, and A. Alù, Optomechanical frequency combs, *New J. Phys.* **20**, 043013 (2018).
- [30] H. Xiong, L.-G. Si, X.-Y. Lü, X.-X. Yang, and Y. Wu, Review of cavity optomechanics in the weak-coupling regime: From linearization to intrinsic nonlinear interactions, *Sci. China Phys. Mech. Astron.* **58**, 1 (2015).
- [31] L.-Y. He, Parity-time-symmetry-enhanced sideband generation in an optomechanical system, *Phys. Rev. A* **99**, 033843 (2019).
- [32] P. Djourwe, J. Y. Effa, and S. G. Nana Engo, Multistability, staircases, and optical high-order sideband combs in optomechanics, *J. Opt. Soc. Am. B* **37**, A36 (2020).
- [33] T. Carmon, H. Rokhsari, L. Yang, T. J. Kippenberg, and K. J. Vahala, Temporal Behavior of Radiation-Pressure-Induced Vibrations of an Optical Microcavity Phonon Mode, *Phys. Rev. Lett.* **94**, 223902 (2005).
- [34] L. Mercadé, L. L. Martín, A. Griol, D. Navarro-Urrios, and A. Martínez, Microwave oscillator and frequency comb in a silicon optomechanical cavity with a full phononic bandgap, *Nanophotonics* **9**, 3535 (2020).
- [35] T. Carmon, M. C. Cross, and K. J. Vahala, Chaotic Quivering of Micron-Scaled On-Chip Resonators Excited by Centrifugal Optical Pressure, *Phys. Rev. Lett.* **98**, 167203 (2007).
- [36] L. Bakemeier, A. Alvermann, and H. Fehske, Route to Chaos in Optomechanics, *Phys. Rev. Lett.* **114**, 013601 (2015).
- [37] F. Monifi, J. Zhang, Ş. K. Özdemir, B. Peng, Y. Liu, F. Bo, F. Nori, and L. Yang, Optomechanically induced stochastic resonance and chaos transfer between optical fields, *Nat. Photonics* **10**, 399 (2016).
- [38] D. Navarro-Urrios, N. E. Capuj, M. F. Colombano, P. D. Garcia, M. Sledzinska, F. Alzina, A. Griol, A. Martinez, and C. M. Sotomayor-Torres, Nonlinear dynamics and chaos in an optomechanical beam, *Nat. Commun.* **8**, 14965 (2017).
- [39] F. Marino and F. Marin, Chaotically spiking attractors in suspended-mirror optical cavities, *Phys. Rev. E* **83**, 015202 (R) (2011).
- [40] H. Rokhsari, T. J. Kippenberg, T. Carmon, and K. J. Vahala, Radiation-pressure-driven micro-mechanical oscillator, *Opt. Express* **13**, 5293 (2005).
- [41] T. Carmon and K. J. Vahala, Modal Spectroscopy of Optoexcited Vibrations of a Micron-Scale On-Chip Resonator at Greater than 1 GHz Frequency, *Phys. Rev. Lett.* **98**, 123901 (2007).
- [42] T. O. Rocheleau, A. J. Grine, K. E. Grutter, R. A. Schneider, N. Quack, M. C. Wu, and C. T.-C. Nguyen, Enhancement of mechanical Q for low phase noise optomechanical oscillators, in *IEEE 26th International Conference on Micro Electro Mechanical Systems (MEMS), 2013, Taipei* (IEEE, New York, 2013), pp. 118–121.
- [43] X. Luan *et al.*, An integrated low phase noise radiation-pressure-driven optomechanical oscillator chipset, *Sci. Rep.* **4**, 6842 (2014).
- [44] T. Carmon, L. Yang, and K. J. Vahala, Dynamical thermal behavior and thermal self-stability of microcavities, *Opt. Express* **12**, 4742 (2004).
- [45] See Supplemental Material at <http://link.aps.org/supplemental/10.1103/PhysRevLett.127.134301> for the details of the theoretical modal, numerical simulations, and other relevant experiment results, which includes Refs. [46–50].
- [46] H. A. Haus, *Waves and Fields in Optoelectronics* (Prentice Hall, New Jersey, 1984).
- [47] G. Anetsberger, R. Rivière, A. Schliesser, O. Arcizet, and T. J. Kippenberg, Ultralow-dissipation optomechanical resonators on a chip, *Nat. Photonics* **2**, 627 (2008).
- [48] M. Hossein-Zadeh, H. Rokhsari, A. Hajimiri, and K. J. Vahala, Characterization of a radiation-pressure-driven

- micromechanical oscillator, *Phys. Rev. A* **74**, 023813 (2006).
- [49] M. Hossein-Zadeh and K. J. Vahala, Observation of optical spring effect in a microtoroidal optomechanical resonator, *Opt. Lett.* **32**, 1611 (2007).
- [50] B. Buscaino, M. Zhang, M. Lončar, and J. M. Kahn, Design of efficient resonant-enhanced electro-optic frequency comb generators, *J. Lightwave Technol.* **38**, 1400 (2020).
- [51] F. Marquardt, J. G. Harris, and S. M. Girvin, Dynamical Multistability Induced by Radiation Pressure in High-Finesse Micromechanical Optical Cavities, *Phys. Rev. Lett.* **96**, 103901 (2006).
- [52] The effective frequency detuning $\Delta\omega_{\text{eff}} = \Delta\omega_L + \Delta\omega_T$ with $\Delta\omega_T = -\alpha_T \bar{D}$ and $\bar{D} = 1/\tau_m \int_t^{t+\tau_m} |a(t)|^2 dt$ being the average energy in one period of the mechanical oscillation ($\tau_m = 2\pi/\Omega_m$).
- [53] V. B. Braginsky and A. B. Manukin, *Measurement of Weak Forces in Physics Experiments* (University of Chicago Press, Chicago, 1977).
- [54] A. G. Krause, J. T. Hill, M. Ludwig, A. H. Safavi-Naeini, J. Chan, F. Marquardt, and O. Painter, Nonlinear Radiation Pressure Dynamics in an Optomechanical Crystal, *Phys. Rev. Lett.* **115**, 233601 (2015).
- [55] F. M. Buters, H. J. Eerkens, K. Heeck, M. J. Weaver, B. Pepper, S. de Man, and D. Bouwmeester, Experimental exploration of the optomechanical attractor diagram and its dynamics, *Phys. Rev. A* **92**, 013811 (2015).
- [56] H. Rokhsari, M. Hossein-Zadeh, A. Hajimiri, and K. Vahala, Brownian noise in radiation-pressure-driven micromechanical oscillators, *Appl. Phys. Lett.* **89**, 261109 (2006).
- [57] The feature of one single series of decay peaks per period originates from the quite small time interval between the two moments with pump detuning crossing zero $\Delta\omega_L + Gx - \beta_T \Delta T = 0$ [Supplemental Material [45], Fig. S6(g)] when the cavity oscillates back and forth, which results in merged optical energy buildup and decay [Supplemental Material [45], Fig. S6(e)] in one oscillation period.
- [58] M. Poot, K. Y. Fong, M. Bagheri, W. H. P. Pernice, and H. X. Tang, Backaction limits on self-sustained optomechanical oscillations, *Phys. Rev. A* **86**, 053826 (2012).
- [59] A. Schliesser, R. Rivière, G. Anetsberger, O. Arcizet, and T. J. Kippenberg, Resolved-sideband cooling of a micromechanical oscillator, *Nat. Phys.* **4**, 415 (2008).
- [60] G. Millot, S. Pitois, M. Yan, T. Hovhannisyan, A. Bendahmane, T. W. Hänsch, and N. Picqué, Frequency-agile dual-comb spectroscopy, *Nat. Photonics* **10**, 27 (2016).
- [61] A. A. Andronov, A. A. Vilt, and S. E. Khaikin, *Theory of Oscillators* (Elsevier, New York, 1966).
- [62] S. M. Link, D. J. H. C. Maas, D. Waldburger, and U. Keller, Dual-comb spectroscopy of water vapor with a free-running semiconductor disk laser, *Science* **356**, 1164 (2017).